Machine learning phase control of filled-aperture coherent beam combining: principle and numerical demonstration

Hongbing Zhou[1,2], Rumao Tao[1,*], Xi Feng[1], Haoyu Zhang[1], Min Li[1], Xiong Xin[1], Yuyang Peng[1], Honghuan Lin[1], Jianjun Wang[1], Lixin Yan[2], Feng Jing[1]

[1] *Laser Fusion Research Center, China Academy of Engineering Physics, Mianyang, China*
[2] *Department of Engineering Physics, Tsinghua University, Beijing, China*

Abstract Machine learning has already shown promising potential in tilled-aperture coherent beam combining (CBC) to achieve versatile advanced applications. By sampling the spatially separated laser array before the combiner and detuning the optical path delays, deep learning techniques are incorporated into filled-aperture CBC to achieve single-step phase control. The neural network is trained with far-field diffractive patterns at defocus plane to establish one-to-one phase intensity mapping, and the phase prediction accuracy is significantly enhanced thanks to the strategies of sin-cos loss function and two-layer output of phase vector that are adopted to resolve the phase discontinuity issue. The results indicate that the trained network can predict phases with improved accuracy, and phase-locking of 9-channel filled-aperture CBC has been numerically demonstrated in a single step with a residual phase of λ/70. To the best of our knowledge, this is the first time that machine learning has been made feasible in filled-aperture CBC laser systems.

This peer-reviewed article has been accepted for publication but not yet copyedited or typeset, and so may be subject to change during the production process. The article is considered published and may be cited using its DOI.

10.1017/hpl.2025.24

Key words: *machine learning; coherent beam combining; phase control*

Correspondence to: R. Tao, Laser Fusion Research Center, China Academy of Engineering Physics, Mianyang 621900, China. Email: supertaozhi@163.com

I. INTRODUCTION

Coherent beam combining (CBC) is one of the most promising techniques for laser power scaling, which can break through the physical limitations of a single beam while maintaining excellent laser characteristics [1-3]. Due to internal and external perturbations, such as spontaneous emission [4], quantum defect [5], environment temperature fluctuation [6], mechanical and acoustical vibrations [7], and so on, laser phases change dynamically in practical operation [8], which severely impairs the combining efficiency and makes the CBC laser system unstable even disable [9]. Active phase control is an efficient solution to phase synchronization and stabilization of multiple lasers in real time, and various control methods have been developed and demonstrated [10-15]. Facilitated by the rapid development of active phase control techniques, several milestones of CBC have been achieved. The maximal average power of 10 kW has been achieved in the ultrashort pulse regimes, while active control of up to 1000 channels has been demonstrated [16, 17]. For some advanced applications, such as laser particle accelerators and coherent amplification networks, higher power and more channels are required [18-23]. Generally, faster active phase control is demanded as the channel number scales, and traditional control methods encounter great challenges in terms of phase-control bandwidth or complexity [24-26].

To further increase the phase-control bandwidth while maintaining simple configuration, machine learning, including reinforcement learning and deep learning, has been applied in the field of CBC phase control [27-32]. Machine learning is a versatile technique that automatically

https://doi.org/10.1017/hpl.2025.24 Published online by Cambridge University Press

learns and extracts complicated features from data, enabling the agent/network to make phase predictions based on system state information such as diffractive patterns or other intensity observations [33, 34]. Direct phase recovery is achievable once the mapping from system state to phase action is established through learning, offering significant advantages of simple optics structure and minimal convergence steps without time-consuming iterations [35]. Theoretically, only one step is required to optimize the phase, which is independent of the number of the channels, making it the most promising control technology for large-scale CBC applications [31, 36]. Deep learning is initially integrated into CBC systems by utilizing non-focal-plane data for training, and 7- and 19-channel CBC phase control is numerically demonstrated with Strehl ratios of 0.98 and 0.84, respectively [37]. 100 channel CBC has been experimentally achieved with a residual phase of $\lambda/30$, which represents the maximal number of beams controlled by machine learning [35]. To date, the majority of applications have focused on tiled-aperture CBC systems [29-32, 35-37]. In contrast, filled-aperture CBC offers the highest combining efficiency as it eliminates energy loss due to sidelobes [38-40], which is particularly crucial for power scaling applications. However, in filled-aperture CBC, all sub-beams overlap completely in both near-field and far-field, resulting in a combined beam pattern that contains minimal phase information, which has limited the utilization of machine learning in filled-aperture CBC. It is noteworthy that machine learning methods typically yield a larger residual phase compared to traditional approaches, prompting researchers to devise a two-stage control scheme to improve accuracy, albeit with increased complexity [28].

In this paper, deep learning algorithm is modified to suppress the residual phase and applied in filled-aperture CBC system with an innovative design in optics structure and control scheme that can achieve phase-locking in a single step with high accuracy. The trained network can

https://doi.org/10.1017/hpl.2025.24 Published online by Cambridge University Press

predict phase with an error of $\lambda/70$ in a single-step for a 9-channel filled-aperture CBC, illustrating the effectiveness of the proposed method. To the best of our knowledge, this represents the first demonstration of machine learning phase control in fill-aperture CBC scenario with high accuracy.

II. PRINCIPLE

A. System Setup

The system structure of filled-aperture CBC based on deep learning phase control is depicted in Fig. 1. The seed laser is split into multiple beam channels by a beam splitter (BS), and each beam path passes through a phase modulator (PM), amplifier, and collimator (CO). All beams are tiled in a dense array, such as square shape [25], hexagon shape [15], or others [41], and are then emitted in the same direction. The laser array is sampled before coming into the filled-aperture beam combiner to obtain the tiled-aperture combined pattern by a camera, which is input into the neural network to make phase prediction and compensate phase noise with high-bandwidth operation. The combiner can take a variety of forms, such as diffractive optical element (DOE) [42], intensity beam splitter based binary tree or segmented mirror [16], and so on, which transforms spatially separated beams into an overlapped beam. The segmented mirror combiner is employed in this paper since it is easy to combine a laser array of linear or square tiling, which will be superimposed into a single beam at one output port if amplitudes match the splitting ratios and phases are locked, and it is only represented by a box in Fig. 1 for simplicity, and its specific architecture can be found in [43]. A liquid crystal (LC) is inserted in the sampled path of each spatially separated beam, so the optical path delays of all beams can be artificially adjusted. The laser array of main power illuminates on the beam combiner and is combined into a single aperture beam in the near-field, and the central intensity of the combined beam is sampled by a

https://doi.org/10.1017/hpl.2025.24 Published online by Cambridge University Press

photodetector (PD), which is used to drive the delay controller and monitor the combining efficiency.

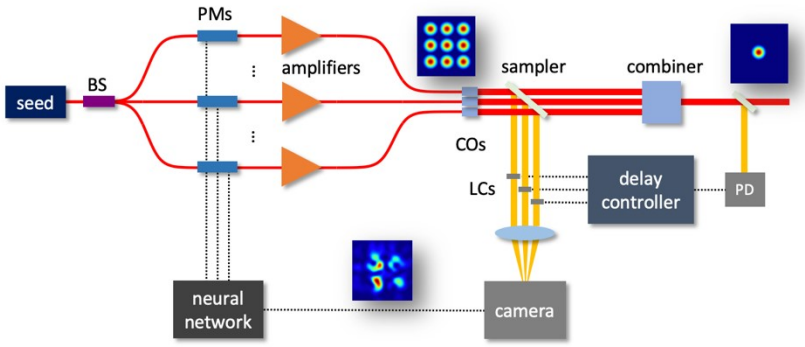

Figure 1. System setup of deep learning phase control for filled-aperture CBC.

As the beam combiner needs to fill the aperture, each beam passes through its own combining route, which results in different optical paths and laser phases. Therefore, the phase relationships at the camera are not consistent with those at the PD due to optical path differences, which accounts for why the delay control is essential to compensate for the static path-related phases. It should be noted that although the optical path difference dominantly occurs inside the combiner, it can be eliminated by adjusting the phase delays in the sampled path instead, which is consistent with high-power operation since the avoidance of manipulation on high-power beams. The delay control is an optimization problem of multiple variables, thus stochastic parallel gradient descent (SPGD) can be employed to address the issue conveniently. The process of delay control can be described in the flow chart of Table 1, where T_p/T_d denotes the time step of phase/delay update, and γ and σ are gain coefficient and perturbation amplitude of SPGD algorithm. As SPGD algorithm requires two-way perturbations before parameter update, one step of delay control is divided into three mini-steps, so the current step of delay control is calculated according to $T_d/3$ as shown in line 4 of Table 1. The phase control is much faster than delay control ($T_p \ll T_d$), so phase-locking is achieved immediately after the delays are perturbed or

https://doi.org/10.1017/hpl.2025.24 Published online by Cambridge University Press

updated. It should be emphasized that PD signal does not change directly with delays of LCs but changes with phases of PMs, since the neural network will dynamically drive PMs to compensate for the delay changes and maintain phase-locking at the camera.

Table 1. Procedure for delay control.

Require: Parameters T_p, T_d, γ, and σ are defined.	
1:	**for** *step* = 1 to ∞ **do**
2:	capture an image and feed into neural network
3:	update phases $\boldsymbol{\varphi} \leftarrow \boldsymbol{\varphi} - \boldsymbol{\varphi}_{pred}$
4:	calculate delay control step $s = step \cdot T_p/(T_d/3)$
5:	**if** (s modulo 3) = 1 **then**
6:	generate random vector $\delta\tau$ of variance σ^2
7:	apply positive perturbation $\boldsymbol{\tau} + \delta\boldsymbol{\tau}$
8:	get PD signal as metric $J_+ = I_{PD}(\tau + \delta\boldsymbol{\tau})$
9:	**else if** (s modulo 3) = 2 **then**
10:	apply negative perturbation $\boldsymbol{\tau} - \delta\boldsymbol{\tau}$
11:	get PD signal as metric $J_- = I_{PD}(\boldsymbol{\tau} - \delta\boldsymbol{\tau})$
12:	**else**
13:	calculate metric change: $\Delta J = (J_+ - J_-)/(J_+ + J_-)$
14:	update delays $\boldsymbol{\tau} \leftarrow \boldsymbol{\tau} + \gamma\delta\boldsymbol{\tau}\Delta J/\sigma^2$
15:	**end if**
16:	**end for**

With the delay control done, the phase relationships at the tiled-aperture path (camera) are the same as the filled-aperture path (PD), thus the filled-aperture combining efficiency will be maximized when laser phases are synchronized at the camera by neural network. Therefore, filled-aperture phase control can be converted into tiled-aperture phase control with proper delay control. In addition, optical path length differences in the combiner are generally piston errors, so the delay control can be implemented in a once and forever manner theoretically, and only phase control is required in the end.

https://doi.org/10.1017/hpl.2025.24 Published online by Cambridge University Press

B. Training Strategies

Although the mapping from combined pattern to laser phases can be interpreted as a pattern recognition problem, there are two barriers to cross when applying deep learning to the phase control of CBC. The first is the phase periodicity induced discontinuity, where φ and $\varphi + 2k\pi$ ($k = 0, \pm1, \pm2, \cdots$) represent the same phase, but their distance is $2k\pi$. In general, phase is limited to a single period $[-\pi, \pi)$ so that every value will correspond to a unique phase, but this does not work well in the training of neural networks as the distance between label and output is usually used to calculate loss. For instance, if the network predicts 0.9π as $-\pi$, the prediction is actually nice because it is equivalent to -1.1π and $-\pi$ with a real distance of 0.1π, but it will result in a large loss due to that the network interprets the distance as 1.9π. To deal with this, a sin-cos loss is introduced and defined as follows

$$L = \frac{1}{2M\left(N-1\right)}\sum_{m=1}^{M}\sum_{n=1}^{N-1}\left[\left|\sin\varphi_n^{(m)} - \sin\varphi_n^{*(m)}\right|^2 + \left|\cos\varphi_n^{(m)} - \cos\varphi_n^{*(m)}\right|^2\right] \tag{1}$$

where φ^* and φ are the true phase and the predicted phase, respectively, and subscribe n denotes the beam number (total is N-1 as one beam is set as reference), and superscript (m) denotes the sample number (total is batch size M).

The proposed loss function calculates both sine and cosine distances between network output and true phase, which is inducive to overcome the aforementioned phase discontinuity since phase is not compared directly. However, if the network is requested to output phase predictions φ, the discontinuity remains unsolved. More specifically, phases of around $-\pi$ and π should be predicted using similar image features with the same network parameters, so the network will struggle to minimize losses at both ends rather than learn an accurate and unique mapping function, which means that the learning problem is not a strict one-to-one mapping

https://doi.org/10.1017/hpl.2025.24 Published online by Cambridge University Press

indeed, so the learning process is not very well. Therefore, the output of the network is designed to consist of both the sine and cosine of phase φ. It should be noted that the sine and cosine values may not strictly satisfy the equation of $\sin^2\varphi + \cos^2\varphi = 1$, as they are predicted independently by the neural network. Letting C and S represent the predicted cosine of phase ($\cos\varphi$) and predicated sine of phase ($\sin\varphi$), although C and S probably correspond to different predicated phases, a more accurate phase prediction φ can be calculated using both C and S by Eq. (2). By doing so, the prediction discontinuity can be solved, as the real part and imaginary part are both continuously varied, and phases of -π and π are positioned in the same line of the complex plane.

$$\varphi = \mathrm{angle}\left(C + iS\right) \tag{2}$$

The other barrier in the application of deep learning phase control is the non-unique phase intensity mapping, which represents that different phase relationships may result in the same intensity distribution of the far field. Many solutions have been developed to solve the non-unique mapping problem, and one of the simplest, diffractive pattern at a slightly defocused plane, is adopted here. In the simulation, all beams are assumed to be Gaussian fundamental mode and linearly polarized at the same direction. The intensity of the combined beam at the defocus far-field can be expressed as

$$I\left(\mathbf{r}, z = L\right) = \frac{1}{i\lambda L}\exp\left(i\frac{\pi r^2}{\lambda L}\right) FT\left\{\exp\left[i\frac{\pi\rho^2}{\lambda}\left(\frac{1}{L} - \frac{1}{f}\right)\right]\sum_{n=0}^{N-1} A\exp\left[-\left(\frac{\boldsymbol{\rho} - \boldsymbol{\rho}_{0n}}{w}\right)^2\right]\exp\left(i\varphi_n\right)\right\} \tag{3}$$

where A, φ, w, $\boldsymbol{\rho}_0$, and λ are the amplitude, phase, waist width, central position, and wavelength of laser, respectively, and $\boldsymbol{\rho}$ and $\mathbf{r}$ are the position vectors at the emission plane and observation

https://doi.org/10.1017/hpl.2025.24 Published online by Cambridge University Press

plane while ρ and r of normal forms represent corresponding scalar distances from the origin. FT{·} refers to Fourier transform, and L and f represent the propagation length and the focus length (in our study, $L \neq f$). It should be pointed out that the strategy of defocus pattern is not contributed in this work, but it is important not only for solving the non-unique mapping problem but also for clarifying the optical model of dataset preparing. Therefore, the advantages of the strategies discussed in the following section correspond to the strategies of sin-cos loss and two-layer output, rather than the defocus pattern since the training dataset is kept the same with or without strategies.

C. Neural Network Construction

VGG model, which is a powerful and prevalent tool in computer vision, is modified and employed as our neural network to achieve CBC phase control [44]. It is a classical convolution neural network, which consists of a serial of convolution layers, max-pooling layers, and fully connected (FC) layers as shown in Fig. 2. For simplicity, the network is divided into 5 blocks, and each block is made up of 1 or more convolution layers followed by a max-pooling layer. Based on the number of convolutional layers, VGG can be named as VGG-11, VGG-13, and so on, and the one used in our study is VGG-16, including 13 convolution layers and 3 FC layers. The kernel size of all convolution layers is 3×3 and the padding size is 1, so the image height and width do not change after convolution, but the channel number might be different depending on the number of convolution filters. The kernel size of max-pooling layers is 2×2, so the image height and width will be reduced to the half after pooling. It should be noted that a ReLU function is followed with each convolution layer and FC layer, which are not shown in the figure. A dropout layer with a possibility of 0.5 is added in both FC1 and FC2 to reduce the

https://doi.org/10.1017/hpl.2025.24 Published online by Cambridge University Press

possibility of overfitting, and the activation function of FC3 is changed from Softmax to Sigmoid as phase prediction is a regression problem rather than a classification problem.

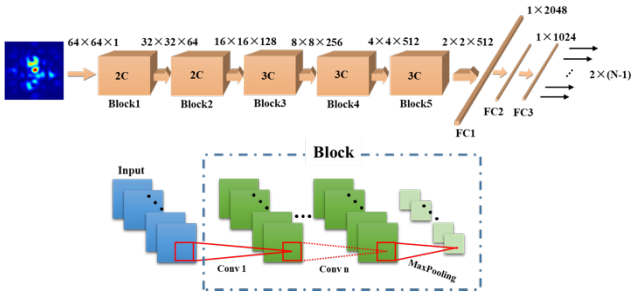

Figure 2. Structure chart of the VGG network.

The built VGG network can extract features of the input intensity profile by convolution operations layer by layer, and it can leave out redundant features by max-pooling layers to prevent overfit. Additionally, the ReLU activation layers are beneficial to enhance the nonlinear expression ability of the network. After a series of convolution and max-pooling layers, the image features are efficiently extracted and condensed, and are flattened and reorganized by the FC layers. Finally, the output layer is formatted in size of $2 \times (N - 1)$ while it is $1 \times (N - 1)$ for traditional network, so it maps these extracted features into the real and imaginary parts of a complex phase vector and makes phase prediction consequently. To accommodate the phase control tasks, the input image size of VGG-11 model is changed to 64×64×1, and the intensity value is normalized with the maximal value being 1.

III. RESULTS

A. Phase prediction with improved accuracy

The modified VGG-16 network for 9-channel CBC is built up and trained with 18,000 labeled data pairs. The batch size is 250 and the epoch is 90, and stochastic gradient descent with momentum term is selected as the optimization algorithm, with a learning rate of 0.05 and momentum factor of 0.9. It costs less than 20 minutes for a personal computer to finish the

https://doi.org/10.1017/hpl.2025.24 Published online by Cambridge University Press

training process. The calculated MSE loss of 1,000 testing samples at every epoch is plotted in Fig. 3. The MSE loss drops from 1.0 at the start to 0.015 at the end, and it can be seen that the loss decreases very fast at the first 5 epochs and gradually keeps stable in the later epochs, illustrating that the network is convergent and the mapping from pattern to phase is constructed.

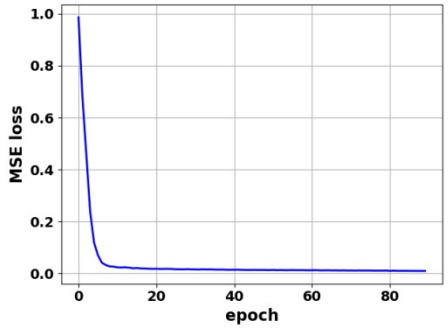

Figure 3. Testing loss with respect to the training epoch.

Then the trained network is validated on 1,000 datasets that are not included in the training and testing process, and the phase predictions are compared with the true labels. Firstly, the root mean square (RMS) residual phase is introduced for quantitative analysis, which is calculated by

$$\varphi_{\mathrm{res}} = \frac{1}{N}\sum_{n=0}^{N-1}\left(\varphi_n - \bar{\varphi}\right)^2,\ \bar{\varphi} = \frac{1}{N}\sum_{n=0}^{N-1}\varphi_n \tag{4}$$

The RMS residual phase describes how well laser phases are synchronized, and a large value stands for poor synchronization. The initial states of laser phases are quite different, and the network predictions on samples of different initial states are shown in Fig. 4, where true phase and predicted phase of each beam are compared one by one (only 8 beams are shown because 1 beam is used as phase baseline). The initial RMS residual phases are 0.7, 1.2, 1.8, and 2.4 rad, respectively, and the neural network makes precise predictions on these samples despite the initial conditions, and no selectivity on beam position is observed as well. If predicted phases are

https://doi.org/10.1017/hpl.2025.24 Published online by Cambridge University Press

used to compensate initial phases, phase-locking will be achieved in a single step, leading to RMS residual phases of $\lambda/88$, $\lambda/83$, $\lambda/67$, and $\lambda/95$ for the 4 samples, respectively.

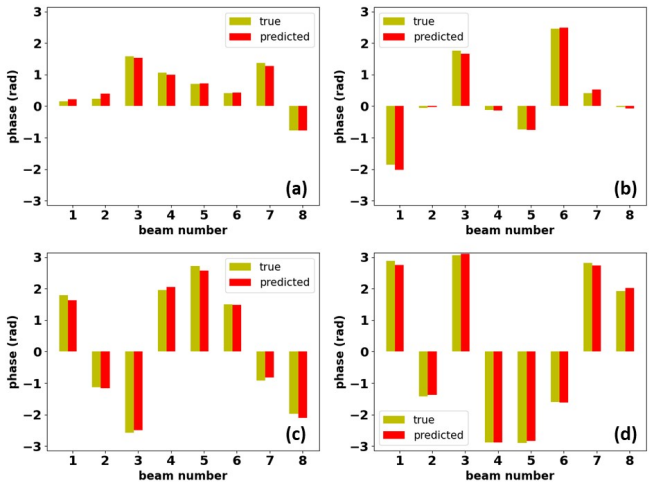

Figure 4. Predicted phase versus true phase for samples of different initial RMS residual phases. (a) 0.7 rad, (b) 1.2 rad, (c) 1.8 rad, and (d) 2.4 rad.

Moreover, the phase prediction of each validation sample is calculated, and compensated phase equals to initial phase minus predicted phase. The compensated phases of the 1,000 validate samples with corresponding initial phases on each beam are plotted in Fig. 5(a), and the dash lines in the middle equal to ± π/20, which is helpful to directly evaluate the prediction accuracy. The phase points in Fig. 5(a) are gathered to a horizontal line with several slight ups and downs, and there are no isolated points far from the dashed area, indicating the network is capable of excellent phase prediction over the full phase range, thus one-step phase control can be implemented no matter what initial phases are. The RMS residual phase after one-step compensation averaged on the sample number is $\lambda/95$, which shows high prediction accuracy of our network. In addition, the same network is trained with the same dataset and same epochs using traditional MSE loss, and the phase compensation performance is shown in Fig. 5 (b). It is obviously that the accuracy is much worse, especially when initial phases are close to ±π, and the

https://doi.org/10.1017/hpl.2025.24 Published online by Cambridge University Press

average residual phase after one-step control is only $\lambda/12$, showing great advantages of the proposed training strategies.

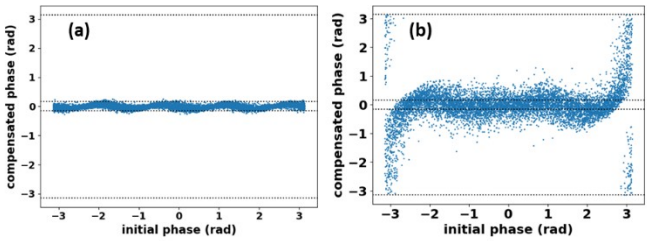

Figure 5. Prediction error as a function of true phase. (a) Cos-sin loss and two-layer output. (b) Traditional MSE loss and one-layer output.

B. Single-step phase control in filled aperture system

Based on the trained neural network, single-step phase control is implemented in filled-aperture CBC system with the assist of delay control. The control procedure is described before in Table 1 in detail, and the active control simulations are carried out in the whole phase and delay feedback loop. The parameters of SPGD algorithm for delay control are optimized as $\gamma = 0.6$ and $\sigma = 0.05$, and the execution speed of deep learning phase control is set to be 10 times as the delay loop, so the phases are locked when the delay controller acts and loop crosstalk will be avoided. The power in bucket (PIB) of the far-field pattern at the focus plane is calculated at each step to monitor the state of the sampled beam, and the PD signal represents the combining efficiency of the whole system. PIB and PD signal intensity during the process of phase-delay are shown in Fig. 6, where the x-label represents the delay control step. The drop-off lines in Fig. 6(a) correspond to the voltage perturbations and updates of LCs, and combining efficiencies of both filled and tiled aperture beams are maximized after around 35 steps. This result demonstrates that delay control is effective and single-step phase control for filled-aperture CBC is feasible.

https://doi.org/10.1017/hpl.2025.24 Published online by Cambridge University Press

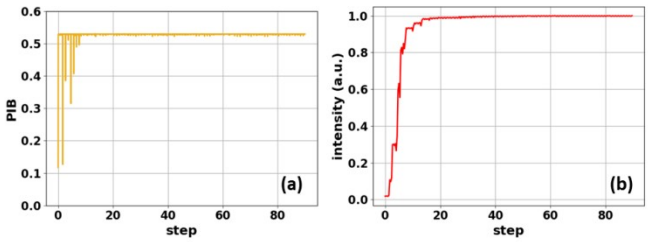

Figure 6. System state variation during delay control process. (a) PIB of the tiled-aperture combined beam. (b) Normalized intensity of filled-aperture combined beam.

Therefore, the phase relationships between tiled and filled aperture beams are synchronized after delay control, and phase control can be implemented directly in the fill-aperture CBC with delay value fixed. The delay residual after control of Fig. 6 is $\lambda/101$ (converted to phase residual), which is small enough and is expected to have no significant impact on the control performance as the achieved combining efficiency is very close to 100% in Fig. 6(b). This delay residual is considered in the simulation while the real-time delay control is turned off, and the results of 20 random initial states are shown in Fig. 7. One can clearly see that the system reaches the maximal intensity in a single step from any initial states. The combining efficiency is 98.7% and the residual phase is $\lambda/70$, which is limited by the delay control residual. Moreover, filled-aperture CBC is implemented by the traditional network as well, the combining efficiency over 20 random cases is 79.2% on average, showing great improvement brought by the training strategies.

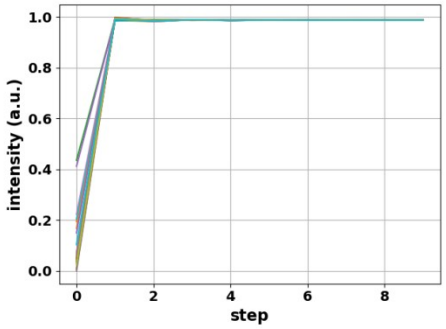

Figure 7. Single-step phase control of filled-aperture CBC

https://doi.org/10.1017/hpl.2025.24 Published online by Cambridge University Press

As mentioned in section 2.A, phase control performance is critical for delay control, which will determine the feasibility of filled-aperture CBC by deep learning. Therefore, the requirement on phase prediction accuracy with application to filled-aperture CBC is investigated. Neural network with different prediction accuracy is obtained by varying training epochs, and the results are shown in Fig. 8. It is apparent that one-step phase residual decreases rapidly as training epochs increase, and the filled-aperture combining efficiency by using the neural network in cooperation with delay controller becomes higher at the same time. For a typical efficiency of 95%, one-step residual phase of the neural network should be better than $\lambda/50$.

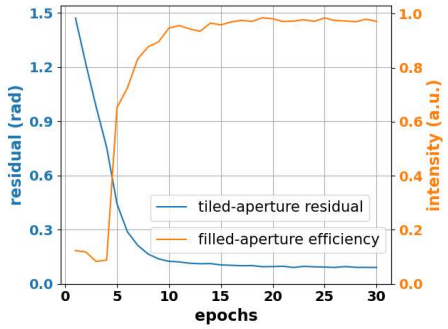

Figure 8. Single-step residual phase for filled-aperture CBC and combining efficiency for tilled-aperture CBC with respect to training epochs

Another important issue is the dynamic phase perturbations that are commonly encountered in a real laser system. Bandwidth-limited white noise is introduced in the simulation model [22], where the noise cut-off frequency is set to be 100 Hz and RMS amplitude is $\lambda/30$. The time domain phase drift of one of the lasers is exemplified in Fig. 9(a), and each laser experiences independent phase perturbations with the same cut-off frequency and RMS amplitude. The execution rate of deep learning algorithm is set as 1 kHz (single-step time of 1 ms), and filled-aperture combining efficiency from open and closed loop is illustrated in Fig. 9(b). With the control loop on, combining efficiency rises immediately from less than 10% in open loop to 96.7% in closed loop. More specifically, the transition process at the moment of control turning

https://doi.org/10.1017/hpl.2025.24 Published online by Cambridge University Press

on is shown in Fig. 9(c), and it manifests that phase-locking is achieved in a single-step (1 ms) even with dynamic phase noise. Therefore, the dynamic phase noise does not affect the time convergence, but leads to a reduced efficiency loss (from 98.7% to 96.7%) and an increased residual phase (from $\lambda/70$ to $\lambda/36$). As the control loop takes actions at a step of 1 ms, the combining efficiency is slowly drift within the relaxation time before next phase action is implemented. Power spectral density of phase noise of one laser is plotted in Fig. 9(d), indicating that phase noise below 1 kHz is suppressed, and the control bandwidth of 1 kHz is achieved in a 1 kHz control loop thanks to the single-step advantage. It is prospected that the control bandwidth will be further improved using a faster control loop.

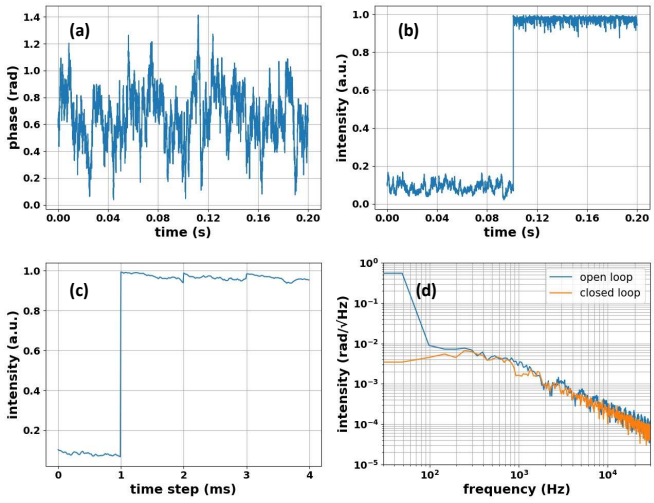

Figure 9. Filled-aperture CBC with dynamic phase noise. (a) Time-dependent phase noise. (b) Combining efficiency in open and closed loop. (b) Time convergence detail from open to closed loop. (d) Phase noise spectrums in open and closed loop.

IV. Discussion

One of the most attractive advantages of deep learning phase control lines in that phase-locking can be achieved in a single step in spite of increasing channels. Indeed, phase control

https://doi.org/10.1017/hpl.2025.24 Published online by Cambridge University Press

performance highly depends on the residual phase or prediction error of the neural network, and previous studies manifested decreasing accuracy with increasing channel number [37], so it is important to find out whether channel number affects the residual phase in our models.

Neural networks for 9, 16, 25, and 36 beams are constructed and trained using the same strategies aforementioned, with dataset size of 2,000 times of beam number and training epoch 10 times of beam number, as explicated in Table 2. The network structure is VGG-16 as described before, but the output number is varied with beam number. The average residual phases after one-step correction in filled-aperture systems with different channels are listed in Table 2. It is indicated that the residual phase increases as channel scales, but the accuracy for a 36-channel CBC system is $\lambda/21$ and the combining efficiency is higher than 90%, which is acceptable for typical applications. On the contrary, for traditional network without using the proposed strategies, the one-step residual phase is about $\lambda/4$ for 16 or more channels, and the combining efficiencies are less than 5% for these cases. In the presence of dynamic perturbations (noise properties the same as the 9-channel), filled-aperture CBC of 36 channels controlled by deep learning is simulated as well, and the results are shown in Fig. 10. It is indicated that convergence speed is not affected by the dynamic noise, but the combining efficiency gets worse in closed loop, which is about 81%. On the contrary, neural network without training strategies is simulated as well, resulting in a combining efficiency of only 2%, showing no improvement by phase control. The other issue to be concerned is that the dataset size and training time rise rapidly with channel number, as shown in Table2, which is due to that the phase relationships and diffraction patterns become far more complicated. In specific, if laser phase is divided into p discrete pieces, such as p values equally spacing in the range of $[-\pi, \pi]$, the permutation and combination of N lasers will be p^N, which means the problem dimension increases exponentially

https://doi.org/10.1017/hpl.2025.24 Published online by Cambridge University Press

with channel number N. To acquire a higher accuracy, the number of phase pieces p should be larger, which will lead to a much larger dimension expansion rate. Therefore, the linearly increasing dataset size cannot catch up with the problem complexity, thus the residual phase for a larger array becomes worse to some extent. In addition, the one-step time of network prediction is given in Table 2 as well, showing that control speed is not affected by channel numbers, and the one-step time is close to 1 ms.

Table 2. Residual phase after one-step phase control for different channel numbers.

N	9	16	25	36
dataset size	18,000	32,000	50,000	72,000
train epochs	90	160	250	360
train time / h	0.60	1.86	4.52	9.37
one-step time / ms	1.1	1.1	1.0	1.0
φ_{res} of this network	λ/70	λ/43	λ/27	λ/21
φ_{res} of traditional network	λ/12	λ/4	λ/4	λ/4

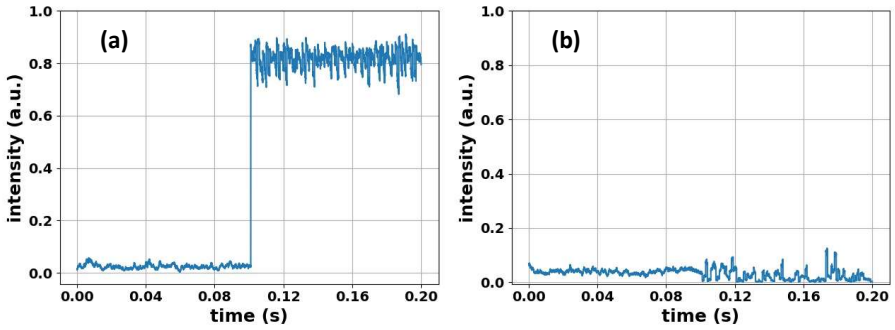

Figure 10. Filled-aperture CBC of 36 channels with dynamic phase noise. Phase control by deep learning (a) with and (b) without strategies.

In our simulation, the network is not optimized for different system scales, it can be speculated that a smaller residual phase is possible at the price of a deeper and larger network and more efforts on training. For instance, if the dataset size of 36-channel CBC is supplemented be the twice (144,000), the residual phase of filled-aperture control after one step will be improved to be λ/29. Although more time and efforts are spent in the network training for a

https://doi.org/10.1017/hpl.2025.24 Published online by Cambridge University Press

larger array, the accuracy is still worse than the 9-channel case. Therefore, to apply the method on a large-scale system, other phase-intensity mapping schemes, such as sparsely sampled speckle pattern after a diffuser [35], diffraction pattern of a two-dimensional diffractive optical element [34], and other innovative setups, are desirable to simplify the learning task so that a smaller network can be employed and the training process will be less intractable [30, 45]. In addition, the design and optimization of the dataset will probably make a difference since the randomly generated samples of limited size are impossible to cover the problem space, and most samples will be far from the phase-locking state according to the statistical theorem. Therefore, the channel scalability of our method is related to the design of optical mapping and network structure.

V. CONCLUSION

Deep learning algorithm for phase control of filled-aperture CBC is proposed and verified in a 9-channel system. By accommodating the mapping problem of pattern to phases, the modified neural network employing strategies of sin-cos loss and complex output yields single-step phase compensation with residual phase error as low as $\lambda/95$. The modified deep learning algorithm is then applied to the filled-aperture phase control assisted by delay control, and phase-locking can be achieved in a single step, resulting in a residual phase of $\lambda/70$. Furthermore, the scalability and performance under dynamic phase perturbations of deep learning phase control are discussed, and the results can offer a promising solution to bandwidth improvement for filled-aperture CBC.

References

https://doi.org/10.1017/hpl.2025.24 Published online by Cambridge University Press

1. A. Klenke, M. Müller, H. Stark, M. Kienel, C. Jauregui, A. Tünnermann, and J. Limpert, "Coherent Beam Combination of Ultrafast Fiber Lasers," IEEE J. Sel. Top. Quantum Electron. **24**, 0902709 (2018).
2. Z. Liu, X. Jin, R. Su, P. Ma, and P. Zhou, "Development status of high power fiber lasers and their coherent beam combination," Sci. China Inform. Sci. **62**, 041301 (2019).
3. H. Fathi, M. Närhi, and R. Gumenyuk, "Towards Ultimate High-Power Scaling: Coherent Beam Combining of Fiber Lasers," Photonics **8**, 566 (2021).
4. Y. Li, Z. Fu, L. Zhu, J. Fang, H. Zhu, J. Zhong, P. Xu, X. Chen, J. Wang, and M. Zhan, "Laser frequency noise measurement using an envelope-ratio method based on a delayed self-heterodyne interferometer," Opt. Commun. **435**, 244-250 (2019).
5. H. Tünnermann, J. Neumann, D. Kracht, and P. Weßels, "Gain dynamics and refractive index changes in fiber amplifiers: a frequency domain approach," Opt. Express **20**, 13539-13550 (2012).
6. O. Llopis, P. H. Merrer, H. Brahimi, K. Saleh, and P. Lacroix, "Phase noise measurement of a narrow linewidth CW laser using delay line approaches," Opt. Lett. **36**, 2713-2715 (2011).
7. L. Lombard, G. Canat, A. Durecu, and P. Bourdon, "Coherent beam combining performance in harsh environment," in *Proceedings of Fiber Lasers XI: Technology, Systems, and Applications,* (SPIE, 2014), p. 896107.
8. H. Zhou, R. Tao, H. Zhang, L. Xie, X. Feng, J. Wen, Q. Chu, H. Lin, J. Wang, L. Yan, and F. Jing, "Robust laser phase noise measurement by integration heterodyne for coherent beam combining applications," Opt. Express **32**, 28868 (2024).
9. S. J. Augst, T. Y. Fan, and A. Sanchez, "Coherent beam combining and phase noise measurements of ytterbium fiber amplifiers," Opt. Lett. **29**, 474 (2004).
10. M. Antier, J. Bourderionnet, C. Larat, E. Lallier, E. Lenormand, J. Primot, and A. Brignon, "kHz Closed Loop Interferometric Technique for Coherent Fiber Beam Combining," IEEE J. Sel. Top. Quantum Electron. **20**, 0901506 (2014).
11. R. Su, Z. Zhang, P. Zhou, Y. Ma, X. Wang, and X. Xu, "Coherent Beam Combining of a Fiber Lasers Array Based on Cascaded Phase Control," IEEE Photon. Technol. Lett. **28**, 2585 (2016).

https://doi.org/10.1017/hpl.2025.24 Published online by Cambridge University Press

12. D. Kabeya, V. Kermene, M. Fabert, J. Benoist, J. Saucourt, A. Desfarges-Berthelemot, and A. Barthelemy, "Efficient phase-locking of 37 fiber amplifiers by phase-intensity mapping in an optimization loop," Opt. Express **25**, 13816 (2017).
13. I. Fsaifes, L. Daniault, S. Bellanger, M. Veinhard, J. Bourderionnet, C. Larat, E. Lallier, E. Durand, A. Brignon, and J. C. Chanteloup, "Coherent beam combining of 61 femtosecond fiber amplifiers," Opt. Express **28**, 20152 (2020).
14. H. Chang, Q. Chang, J. Xi, T. Hou, R. Su, P. Ma, J. Wu, C. Li, M. Jiang, Y. Ma, and P. Zhou, "First experimental demonstration of coherent beam combining of more than 100 beams," Photon. Res. **8**, 1943 (2020).
15. P. Ma, H. Chang, Y. Ma, R. Su, Y. Qi, J. Wu, C. Li, J. Long, W. Lai, Q. Chang, T. Hou, P. Zhou, and J. Zhou, "7.1 kW coherent beam combining system based on a seven-channel fiber amplifier array," Opt. Laser Technol. **140**, 107016 (2021).
16. M. Müller, C. Aleshire, A. Klenke, E. Haddad, F. Légaré, A. Tünnermann, and J. Limpert, "10.4 kW coherently combined ultrafast fiber laser," Opt. Lett. **45**, 3083 (2020).
17. Q. Chang, Z. Gao, Y. Deng, S. Ren, P. Ma, R. Su, Y. Ma, and P. Zhou, "Over one thousand fiber laser beams coherent combining under strong noise," Chin. J. Lasers **50**, 0616001 (2023).
18. G. Mourou, B. Brocklesby, T. Tajima, and J. Limpert, "The future is fibre accelerators," Nat. Photonics **7**, 258 (2013).
19. R. Soulard, M. N. Quinn, T. Tajima, and G. Mourou, "ICAN: A novel laser architecture for space debris removal," Acta Astronaut. **105**, 192 (2014).
20. B. Esmiller, C. Jacquelard, H. A. Eckel, and E. Wnuk, "Space debris removal by ground-based lasers: main conclusions of the European project CLEANSPACE," Appl. Opt. **53**, I45 (2014).
21. L. C. Pieters and R. Noomen, "Space-based laser ablation for space debris removal," in *Proceedings of 8th European Conference on Space Debris (virtual)*, T. Flohrer, S. Lemmens and F. Schmitz, ed. (Darmstadt, Germany, 2021).
22. S. Breitkopf, T. Eidam, A. Klenke, L. von Grafenstein, H. Carstens, S. Holzberger, E. Fill, T. Schreiber, F. Krausz, A. Tünnermann, I. Pupeza, and J. Limpert, "A concept for multiterawatt fibre lasers based on coherent pulse stacking in passive cavities," Light Sci. Appl. **3**, e211 (2014).

https://doi.org/10.1017/hpl.2025.24 Published online by Cambridge University Press

23. G. Mourou, "Science and applications of the coherent amplifying network (CAN) laser," Eur. Phys. J. Spec. Top. **224**, 2527 (2015).
24. P. Zhou, Z. J. Liu, X. L. Wang, Y. X. Ma, H. T. Ma, X. J. Xu, and S. F. Guo, "Coherent Beam Combining of Fiber Amplifiers Using Stochastic Parallel Gradient Descent Algorithm and Its Application," IEEE J. Sel. Top. Quantum Electron. **15**, 248 (2009).
25. J. Bourderionnet, C. Bellanger, J. Primot, and A. Brignon, "Collective coherent phase combining of 64 fibers," Opt. Express **19**, 17053 (2011).
26. H. Zhou, X. Feng, L. Xie, M. Li, H. Zhang, R. Tao, H. Lin, J. Wang, L. Yan, and F. Jing, "Comprehensive investigation of LOCSET and SPGD algorithms in coherent beam combining applications," Opt. Laser Technol. **181**, 111568 (2025).
27. H. Tunnermann and A. Shirakawa, "Deep reinforcement learning for coherent beam combining applications," Opt. Express **27**, 24223 (2019).
28. T. Hou, Y. An, Q. Chang, P. Ma, J. Li, L. Huang, D. Zhi, J. Wu, R. Su, Y. Ma, and P. Zhou, "Deep-learning-assisted, two-stage phase control method for high-power mode-programmable orbital angular momentum beam generation," Photon. Res. **8**, 715 (2020).
29. J. Zuo, H. Jia, C. Geng, Q. Bao, F. Zou, Z. Li, J. Jiang, F. Li, B. Li, and X. Li, "Deep Learning Piston Aberration Control of Fiber Laser Phased Array By Spiral Phase Modulation," J. Lightwave Technol. **40**, 3980 (2022).
30. M. Shpakovych, G. Maulion, A. Boju, P. Armand, A. Barthélémy, A. Desfarges-Berthelemot, and V. Kermene, "On-Demand Phase Control of a 7-Fiber Amplifiers Array with Neural Network and Quasi-Reinforcement Learning," Photonics **9**, 243 (2022).
31. Y. Xie, F. Chernikov, B. Mills, Y. Liu, M. Praeger, J. A. Grant-Jacob, and M. N. Zervas, "Single-step phase identification and phase locking for coherent beam combination using deep learning," Sci. Rep. **14**, 7501 (2024).
32. W. Jiang, J. Gao, G. Tan, M. Zhang, J. Dou, J. Di, and Y. Qin, "High environmentally adaptable phase control with reinforcement learning for coherent beam combination," Opt. Lasers Eng. **183**, 108534 (2024).
33. H. Tünnermann and A. Shirakawa, "Deep reinforcement learning for tiled aperture beam combining in a simulated environment," J. Phys. Photonics **3**, 015004 (2021).
34. D. Wang, Q. Du, T. Zhou, D. Li, and R. Wilcox, "Stabilization of the 81-channel coherent beam combination using machine learning," Opt. Express **29**, 5694 (2021).

https://doi.org/10.1017/hpl.2025.24 Published online by Cambridge University Press

35. M. Shpakovych, G. Maulion, V. Kermene, A. Boju, P. Armand, A. Desfarges-Berthelemot, and A. Barthélemy, "Experimental phase control of a 100 laser beam array with quasi-reinforcement learning of a neural network in an error reduction loop," Opt. Express **29**, 12307 (2021).
36. B. Mills, J. A. Grant-Jacob, M. Praeger, R. W. Eason, J. Nilsson, and M. N. Zervas, "Single step phase optimisation for coherent beam combination using deep learning," Sci. Rep. **12**, 5188 (2022).
37. T. Hou, Y. An, Q. Chang, P. Ma, J. Li, D. Zhi, L. Huang, R. Su, J. Wu, Y. Ma, and P. Zhou, "Deep-learning-based phase control method for tiled aperture coherent beam combining systems," High Power Laser Sci. Eng. **7**, e59 (2019).
38. S. M. Redmond, D. J. Ripin, C. X. Yu, S. J. Augst, T. Y. Fan, P. A. Thielen, J. E. Rothenberg, and G. D. Goodno, "Diffractive coherent combining of a 2.5 kW fiber laser array into a 1.9 kW Gaussian beam," Opt. Lett. **37**, 2832 (2012).
39. F. Angel, D. Iyad, H. H. Roger, E. Thomas, and T. A. Brian, "Multi-kilowatt diffractive coherent combining of pseudorandom-modulated fiber amplifiers," Opt. Eng. **55**, 096101 (2016).
40. Z. J. Liu, P. F. Ma, R. T. Su, R. M. Tao, Y. X. Ma, X. L. Wang, and P. Zhou, "High-power coherent beam polarization combination of fiber lasers: progress and prospect [Invited]," J. Opt. Soc. Am. B **34**, A7 (2017).
41. W. Li, J. Liao, Y. Gao, Y. Sun, Y. Tan, Z. Wang, and J. Lan, "Coherent beam combining array arrangement with a large number of elements," Opt. Commun. **522**, 128687 (2022).
42. P. A. Thielen, J. G. Ho, D. A. Burchman, G. D. Goodno, J. E. Rothenberg, M. G. Wickham, A. Flores, C. A. Lu, B. Pulford, C. Robin, A. D. Sanchez, D. Hult, and K. B. Rowland, "Two-dimensional diffractive coherent combining of 15 fiber amplifiers into a 600 W beam," Opt. Lett. **37**, 3741 (2012).
43. C. Aleshire, A. Steinkopff, C. Jauregui, A. Klenke, A. Tünnermann, and J. Limpert, "Simplified design of optical elements for filled-aperture coherent beam combination," Opt. Express **28**, 21035-21045 (2020).
44. K. Simonyan and A. Zisserman, "Very Deep Convolutional Networks for Large-Scale Image Recognition," arXiv:1409.1556 (2015).

https://doi.org/10.1017/hpl.2025.24 Published online by Cambridge University Press

45. D. Wang, Q. Du, T. Zhou, A. Gilardi, M. Kiran, B. Mohammed, D. Li, and R. Wilcox, "Machine Learning Pattern Recognition Algorithm With Applications to Coherent Laser Combination," IEEE J. Quantum Electron. **58**, 6100309 (2022).

https://doi.org/10.1017/hpl.2025.24 Published online by Cambridge University Press